



# Heterogeneous sono-Fenton-like process using nanostructured pyrite prepared by Ar glow discharge plasma for treatment of a textile dye



Alireza Khataee<sup>a,\*</sup>, Peyman Gholami<sup>a</sup>, Behrouz Vahid<sup>b</sup>

<sup>a</sup> Research Laboratory of Advanced Water and Wastewater Treatment Processes, Department of Applied Chemistry, Faculty of Chemistry, University of Tabriz, 51666-16471 Tabriz, Iran  
<sup>b</sup> Department of Chemical Engineering, Tabriz Branch, Islamic Azad University, 51579-44533 Tabriz, Iran

## ARTICLE INFO

### Article history:

Received 24 August 2015  
 Received in revised form 17 September 2015  
 Accepted 18 September 2015  
 Available online 30 September 2015

### Keywords:

Nanostructures  
 Plasma-treated pyrite  
 Heterogeneous sono-Fenton  
 Ar glow discharge plasma

## ABSTRACT

The plasma-treated pyrite (PTP) nanostructures were prepared from natural pyrite (NP) utilizing argon plasma due to its sputtering and cleaning effects resulting in more active surface area. The NP and PTP were characterized using X-ray diffraction (XRD), Fourier transform infrared spectroscopy (FT-IR), Brunauer–Emmett–Teller (BET) and scanning electron microscopy (SEM) methods. The performance of the PTP was greater than NP for treatment of Reactive Red 84 (RR84) by the heterogeneous sono-Fenton process. The optimum amounts of main operational parameters were obtained as PTP of 4 g/L, initial dye concentration of 10 mg/L, pH of 5, and ultrasonic power of 300 W after 120 min of reaction time. Also, the effects of enhancers, and inorganic salts and t-butanol as hydroxyl radical scavengers on the degradation efficiency were investigated. Gas chromatography–mass spectroscopy analysis (GC–MS) was applied for detection of some degradation intermediates. Environmentally friendly plasma modification of the NP, in situ production of H<sub>2</sub>O<sub>2</sub> and ·OH radicals, low leached iron concentration and repeated reusability at the milder pH are the significant benefits of the PTP utilization.

© 2015 Elsevier B.V. All rights reserved.

## 1. Introduction

Increases in the variety of compounds generated by human activities have led to a considerable volume of various industrially polluted wastewaters. Conventional wastewater treatments comprising of biological, physical and chemical processes are not effective for the removal of all pollutants from contaminated effluents. In recent years, considerable efforts have been devoted to developing effective, simple and cheap treatment processes to remove pollutants from contaminated aqueous media. Advanced oxidation processes (AOPs) have attracted special attention as promising alternatives to the conventional processes due to the high efficiency for the treatment of wastewater [1,2]. Among AOPs, the Fenton process is an effective and simple treatment method that is extensively used in the degradation of various chemicals from contaminated water sources [3].

Textile industry wastewater has large amounts of organic dyes, which are resistant to the biological methods. Moreover, other physical and chemical processes like adsorption and coagulation merely transfer contaminants to a secondary phase requires more treatment [4]. Hence, it is significant to find effective wastewater

remediation methods like AOPs, which can not only degrade but also mineralize different contaminants without producing secondary waste [5]. Among AOPs, the Fenton and sonication processes are simple and efficient methods which are applied for the mineralization of various contaminants from polluted water sources [3]. Hydroxyl radicals (·OH) as the most powerful oxidizing agent in AOPs, can be generated by the Fenton reaction involving ferrous iron (Eq. (1)) or from water dissociation under ultrasonic irradiation (Eq. (2)) through cavitation phenomenon [6]. After directing ultrasonic waves into a liquid, the cavitation leads to formation, growth, and finally collapse of microbubbles producing high localized temperatures and pressures (hot spot approach) [7]. However, ultrasonic process consumes more time and energy compared to other methods due to the low degradation rate; hence it can be combined with other processes like Fenton process to enhance their efficiency for the wastewater treatment [8].



On the other hand, homogeneous Fenton process can be just performed in acidic condition (pH 3) preventing the iron precipitation; it also needs to risky storage and transportation of hydrogen peroxide (H<sub>2</sub>O<sub>2</sub>). Moreover, recycling of homogeneous catalyst as

\* Corresponding author.

E-mail addresses: [a\\_khataee@tabrizu.ac.ir](mailto:a_khataee@tabrizu.ac.ir), [ar\\_khataee@yahoo.com](mailto:ar_khataee@yahoo.com) (A. Khataee).

well as its separation from the treated wastewater confines the application of Fenton process. Application of heterogeneous Fenton process with no need for catalyst separation and low leached iron is the practical solution to overcome these obstacles [2]. Heterogeneous Fenton catalysts including pyrite [9], magnetite [10], and goethite [11] are used in this process in which superficial solid Fe ions catalyze the production of  $\cdot\text{OH}$ . The pyrite ( $\text{FeS}_2$ ) is the most abundant metal sulfide in nature and nontoxic. It has potential for utilization in the heterogeneous Fenton reaction. The usage of synthesized pyrite has been studied in several wastewater treatment procedures, such as the Fenton and adsorption processes [12,13]. It should be mentioned that the heterogeneous Fenton process has some limitations compared to the homogeneous one including high mass transfer resistance and few active reaction sites. The effective methods to solve these drawbacks are applying nanostructured particles and ultrasonic irradiation [14].

Plasma is ionized gas, which composes of negative and positive ions, electrons and neutral species, which is noticed as the fourth state of matter, which is an environmentally-friendly method to produce various nanostructures for various applications [15]. For instance, non-thermal plasma techniques such as glow discharge, radio frequency, and silent discharge have been used for modification of different catalysts surfaces and enhancement of their efficiencies [16,17]. For example, the plasma treatment alters the activity and surface structure of natural clinoptilolite and synthesized zeolites [16]. The catalytic activity and stability of the Pd/HZSM-5 catalyst improve after plasma treatment [18]. The selectivity for hydrogenation of acetylene increases after using the  $\text{H}_2$ , Ar and  $\text{O}_2$  atmosphere plasma for modified Pd/ $\text{TiO}_2$  catalyst [19]. Glow discharge plasma treated magnetite using oxygen and argon was applied for treatment of an oxazine dye by catalytic ozonation [20].

The aim of this research is to prepare nanostructured pyrite from natural pyrite with the Ar glow discharge plasma for treatment of RR84 synthetic solutions by the heterogeneous sono-Fenton-like process (US/PTP). To the best of our knowledge there is no report for modification of the NP by plasma and also its usage in combination of ultrasonic for treatment of a model textile dye. The characterizations of treated NP were carried out by XRD, FT-IR, BET and SEM methods. The effect of operational parameters including the PTP dosage, initial RR84 concentration, solution pH, ultrasonic power, presence of enhancers, *t*-butanol, and inorganic salts were studied on the degradation efficiency in a series of batch experiments. Degradation intermediates of RR84 were recognized by the GC–MS.

## 2. Experimental procedure

### 2.1. Materials

Natural pyrite was obtained from Morvarid iron mine (Zanjan, Iran). The mono azo dye, Reactive Red 84 was provided from Ciba-Geigy Ltd (Switzerland), which was used as a textile dye for wool and silk. The properties of RR84 are presented in Table 1. Hydrochloric acid (37%), sodium hydroxide (99%) and hydrogen peroxide (30%) were purchased from Merck (Germany). Ethanol was supplied from Jahan Alcohol Teb Co. (Arak, Iran). Distilled water was used throughout the experiments.

### 2.2. Preparation of pyrite nanostructures

Argon glow discharge plasma was utilized to produce pyrite nanostructures from NP. It was crushed by rod and ball milling (Kian Madan Pars Co, Tehran, Iran) to obtain micro-grained pyrite particles. Then, 2 g of the pyrite particles were placed in a plasma

reactor, which comprised of a Pyrex tube, which was sealed with two aluminum bonnets on its both sides. High-voltage direct current (DC) supplied by a DC power source was connected by the aluminum bonnets. Argon gas was pumped within the reactor to bring the pressure to 40 Pa, applying rotary and turbo-molecular pumps. A schematic diagram of the plasma set-up is illustrated in Fig. 1.

### 2.3. Characterization of pyrite nanostructures

An X-ray diffractometer (XRD, D-5000, Siemens, Germany) was applied for identification of the pyrite phase before and after plasma treatment. FT-IR spectra of the NP and PTP were recorded on a Bruker Tensor 27 FT-IR spectrophotometer (Germany) using KBr pellets. The size and morphology of the NP and PTP samples were investigated using a SEM equipped with an EDX microanalysis (MIRA3 FEG-SEM Tescan, Czech). Microstructure Distance Measurement software (Nahamin Pardazan Asia Co., Iran) was applied to determine the size distribution of the structures developed on the surface of the PTP by using of SEM micrographs. The surface area and pore volume of the both samples were measured by nitrogen adsorption/desorption at 77 K using a Gmini series instrument (Nitrometrics, Japan).

The point of zero charge ( $\text{pH}_{\text{PZC}}$ ) of the PTP is a pH value in which the sample does not alter the solution pH.  $\text{pH}_{\text{PZC}}$  was determined based on a procedure explained by Mustafa et al. [21]. Accordingly, 0.2 g of the PTP were added to nine Erlenmeyer flasks containing 40 mL of  $\text{NaNO}_3$  solution (0.1 N), individually. The pH of the prepared suspensions was adjusted to the range of 2–10 by adding of  $\text{HNO}_3$  and  $\text{NaOH}$  solutions using a pH meter (Metrohm, Switzerland). The suspensions were agitated in a shaker incubator (Fannavaran ISH55LD, Iran) at a rate of 175 rpm for 48 h at ambient temperature. Then, the suspension pH was determined as well as the difference between the initial and final pH ( $\Delta\text{pH}$ ).

### 2.4. Heterogeneous sono-Fenton-like process

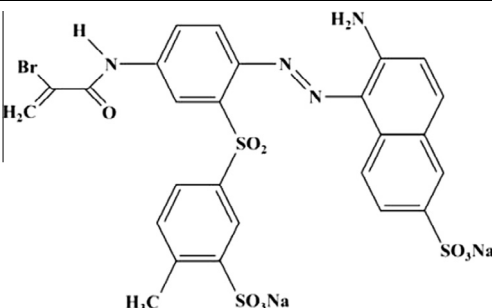
Degradation experiments were performed in a 250 mL Erlenmeyer, which was placed in an ultrasonic bath (EP S3, 40 kHz, 300 W, Sonica, Italy). The distance between the bottom of the reaction vessel and the sonication source was adjusted at 1.0 cm, where the surface of the solution had the maximum turbulence. In general, 100 mL of the RR84 solution with distinct concentration and certain dosage of the PTP were used in all of the experiments. Then, the solution pH was adjusted by adding  $\text{H}_2\text{SO}_4$  (0.1 M) and  $\text{NaOH}$  (0.1 M) and measured by the pH meter to the known values. During the degradation process, the 3 mL of sample was withdrawn with pipette at 15 min reaction intervals. Then the suspended particles were separated completely from the treated solution with a centrifugal separator. The absorbance of the dye solution was measured at the maximum wavelength of the dye ( $\lambda_{\text{max}} = 495 \text{ nm}$ ) using an UV–Vis spectrophotometer (Lightwave S2000, England). An atomic absorption spectroscopy (AAS) apparatus (Novaa 400, Analytikjena, Germany) was used for measurement of the concentration of dissolved iron in the solution. GC–MS analysis was carried out applying a method described in our previous work for identification of the generated degradation intermediate of RR84 during the process [6].

## 3. Results and discussion

### 3.1. Characterization of the PTP

Fig. 2 demonstrates XRD patterns of the NP and PTP samples. In these spectra, peaks were seen at  $2\theta$  values of 28.18, 33.20, 37.22, 40.88, 47.56, 56.38, 59.10, 62.02, and 64.56°, which were attributed

**Table 1**  
Characteristic of RR84.

Name	Chemical structure	Molecular formula	Color index number	$\lambda_{\max}$ (nm)	$M_w$ (g/mol)
Reactive Red 84		$C_{26}H_{19}BrN_4Na_2O_9S_3$	13429	495	753.53

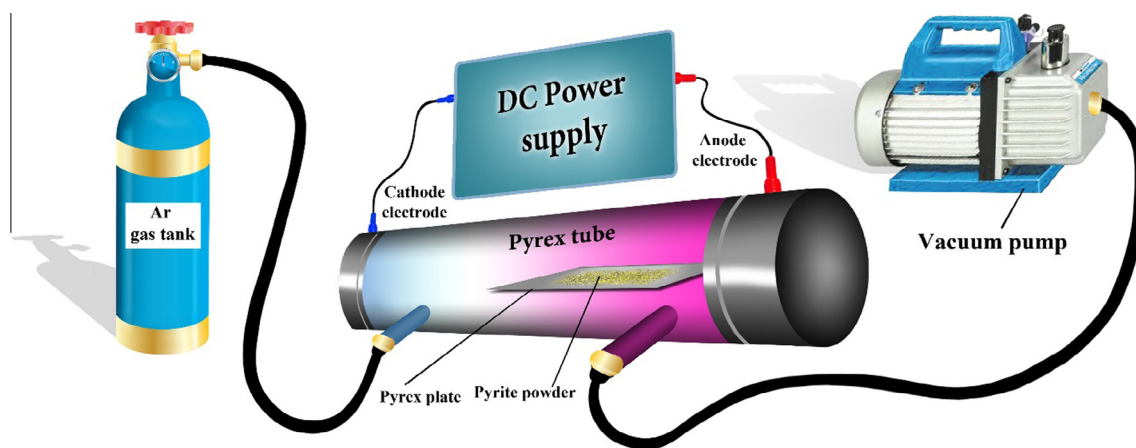


Fig. 1. Schematic diagram of the glow discharge plasma system used in this study.

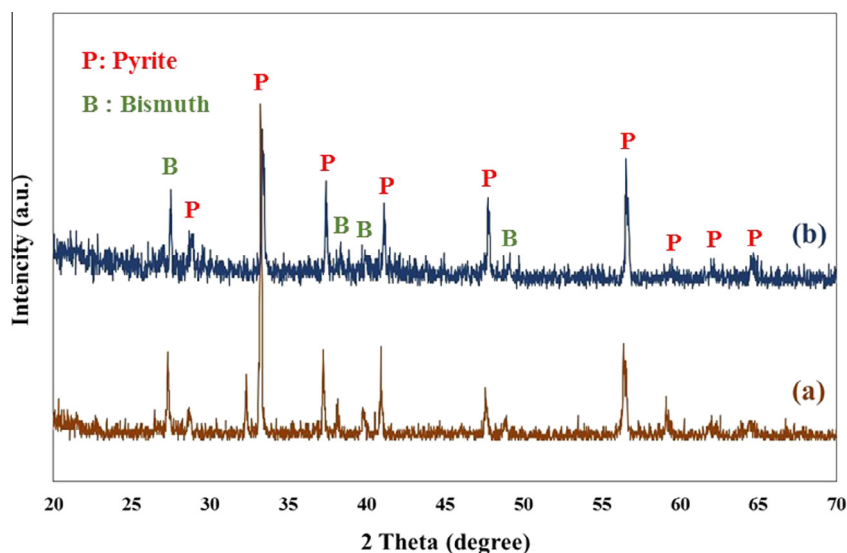


Fig. 2. XRD patterns of (a) NP and (b) PTP samples.

to the characteristic (111), (200), (210), (211), (220), (311), (222), (023), and (321) planes of pyrite (JCPDS card 42-1340), respectively. Comparison between these two spectra and with the standard pyrite pattern confirms that the crystal structure of pyrite, which does not alter by the Ar plasma treatment [21]. Moreover, it seems that the XRD peaks at  $2\theta$  of 27.28, 38.14, 39.72 and 48.88°

relate to the (110), (211), (011) and (200) reflection planes of bismuth [22]. This implies that the presence of bismuth in low quantities in pyrite samples.

FT-IR spectra of the NP and PTP samples are plotted in Fig. 3 In both curves, the peaks of the Fe-S stretching vibration mode (540, 615.2, and 781.1  $\text{cm}^{-1}$ ), the Fe-O-OH vibration (1020.3  $\text{cm}^{-1}$ ), the

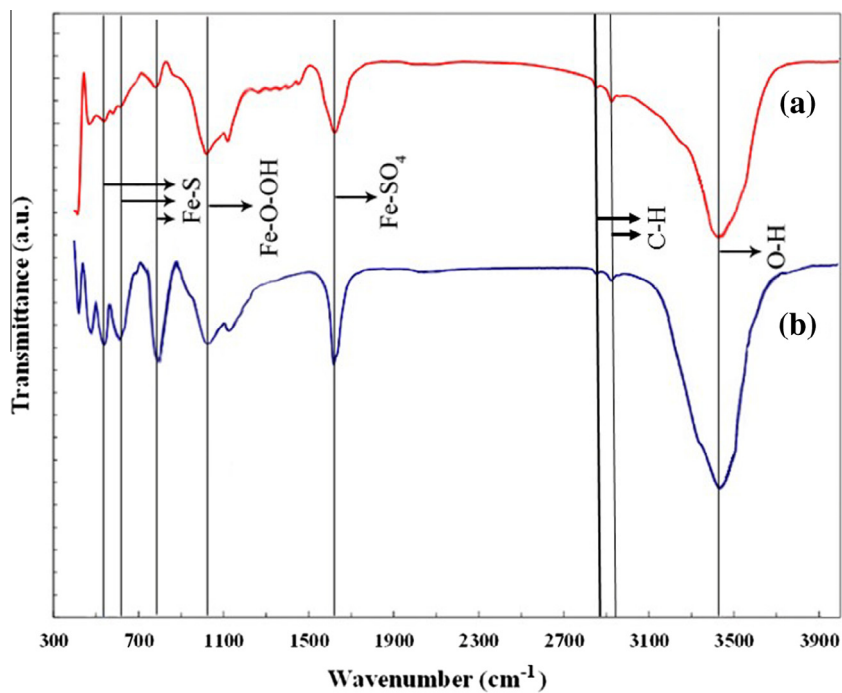


Fig. 3. FT-IR spectra of (a) NP and (b) PTP samples.

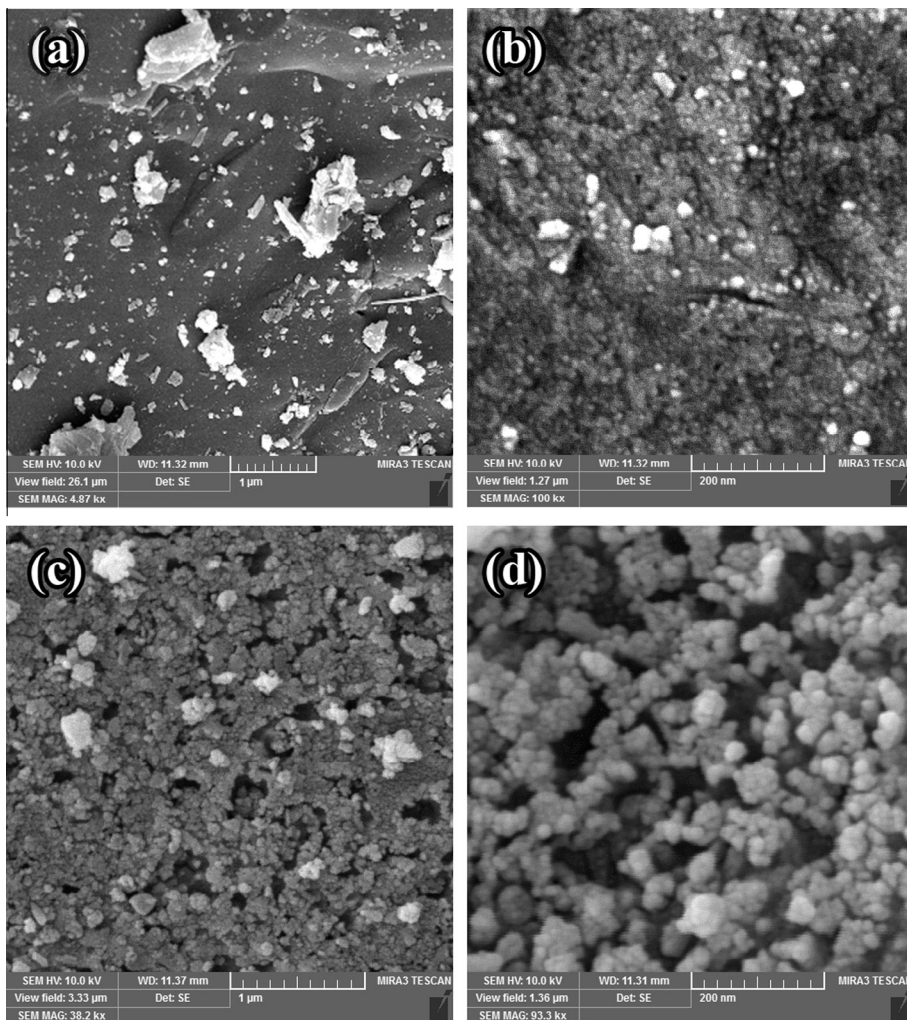


Fig. 4. SEM micrographs of spectra of (a and b) NP and (c and d) PTP samples.

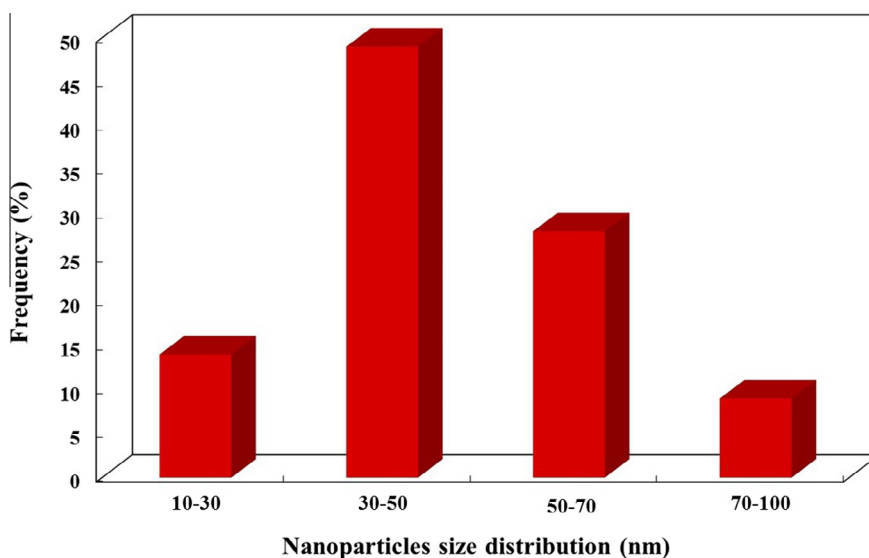


Fig. 5. Particle size distribution of pyrite nanostructures.

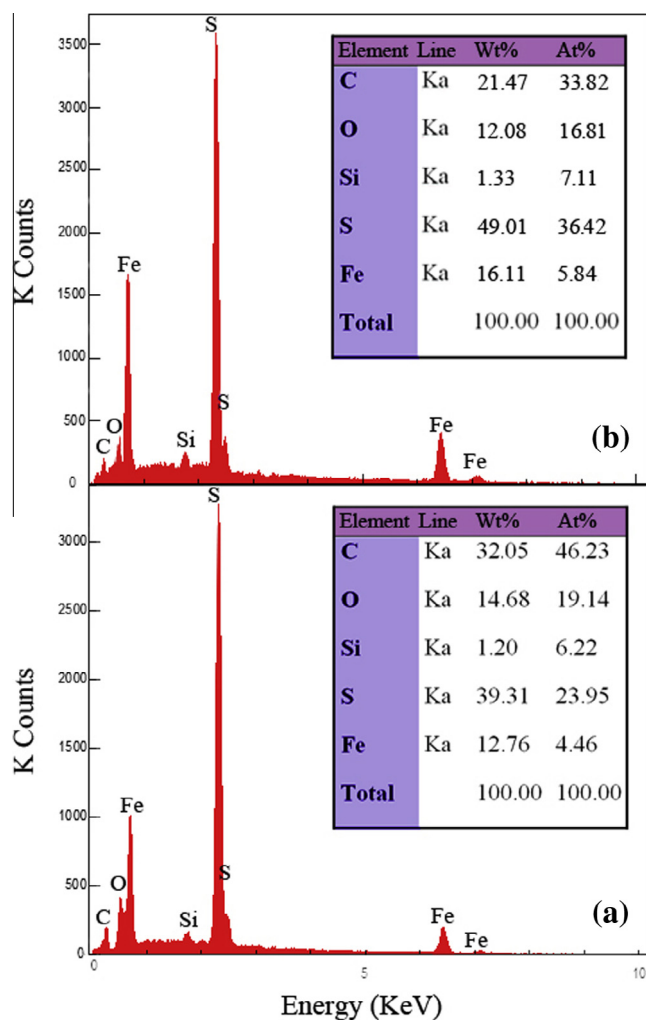


Fig. 6. EDX spectra of (a) NP and (b) PTP samples.

Fe–SO<sub>4</sub> vibration (1623.9 cm<sup>-1</sup>), and the O–H vibration (3450.5 cm<sup>-1</sup>) were found [23,24]. The peaks at 2924 and 2853 cm<sup>-1</sup> are related to the asymmetric and symmetric C–H bonds, respectively [25].

SEM images of the NP and PTP are shown in Fig. 4 with different magnifications. The SEM image of NP (Fig. 4a and b) shows a bulky structure. However, Fig. 4c and d indicate the presence of fine nanostructures in PTP sample. As can be seen in Fig. 5, the average width of these structures is 30–50 nm. Based on the results from the XRD and FT-IR analyses, the Ar plasma treatment does not convert the pyrite to the other material. Comparison of the SEM images for the NP and PTP shows the development of nanostructures on the PTP surface by the plasma treatment. These nanostructures increase the surface area and hence improve the performance of the PTP.

EDX spectra of the NP and PTP samples are shown in Fig. 6a and b, which prove that the main elements such as Fe and S still exist in both of the structures. The weight percent (wt%) of Fe and S elements were found to increase after plasma treatment, which implied some impurities of NP were removed from the pyrite surface [26]. By comparison of curve a (NP) with curve b (PTP) in the FT-IR spectra, the intensity of peaks for the PTP sample were found to be increased. This can also confirm the obtained results from the EDX analysis.

The BET isotherm model was used to analyze the data obtained from the N<sub>2</sub> adsorption/desorption isotherm of NP and PTP. After plasma treatment, the estimated BET surface area and pore volume of the NP were found to be 6.486 m<sup>2</sup>/g and 1.424 cm<sup>3</sup>/g, which increased to 9.652 m<sup>2</sup>/g and 2.199 cm<sup>3</sup>/g, respectively. These enhancements also confirm the development of pyrite nanostructures.

Fig. 7 illustrates the ΔpH change versus the initial pH. When the initial pH of the solution was 6.3, ΔpH was calculated zero, indicating that the net charge of the PTP was zero at this pH. Moreover, when the solution pH was below pHPZC, the PTP surface charge was positive, while it was negatively charged with pH above pHPZC [27].

### 3.2. Comparison of different treatment processes for removal of RR84

The performance of ultrasonic alone and heterogeneous Fenton-like processes using the NP and PTP in the absence and presence of ultrasonic irradiation for the removal of RR84 in aqueous solution were compared to study the effect of Ar plasma treatment and sonication on the NP performance. As can be observed from Fig. 8, after 120 min of treatment, 93.7% degradation occurs applying

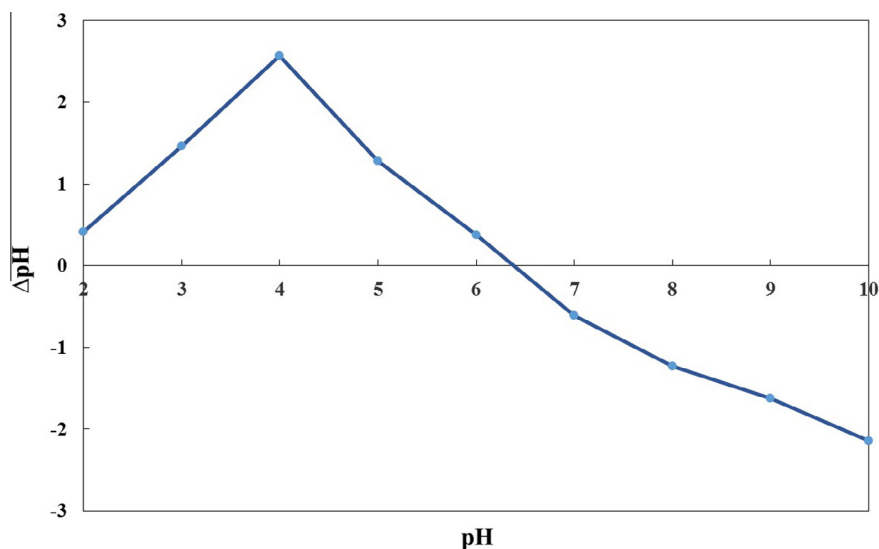


Fig. 7. Plot for determination of PTP  $pH_{pzc}$ .

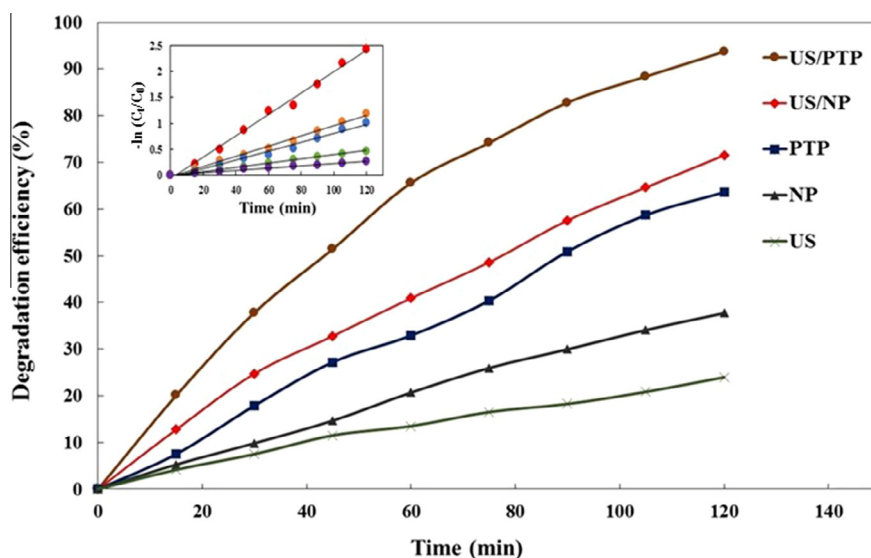
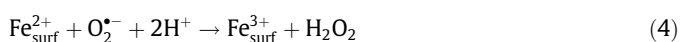


Fig. 8. Comparison of the removal efficiency of RR84 with different processes;  $[RR84]_0 = 10$  mg/L,  $[PTP] = 4$  g/L, ultrasonic power = 300 W, and pH = 5. The inset shows mentioned processes follow pseudo-first order kinetic.

the US/PTP, which was selected to carry out the rest of experiments as the most efficient process.

Nanostructured pyrite is formed under the plasma treatment, which increases the surface area of the NP. Furthermore, the plasma removes some impurities from the surface of the NP, which increased the presence of iron on its surface [28]. Hence, more iron is available for the heterogeneous Fenton-like process to produce in-situ  $H_2O_2$  and  $\cdot OH$  radicals by following reactions on the surface of the PTP [29]:



Then, Fenton reaction can be occurred on the surface of the PTP and in the aqueous solution by  $Fe^{2+}$  ions which are existed in pyrite structure and dissolved in the solution, respectively (Eq. (1)) [9].

Table 2

Effect of the different processes on the apparent pseudo-first order constants of degradation of RR84.

No.	Process	$k_{app}$ ( $min^{-1}$ )	Correlation coefficient ( $R^2$ )
1	US	0.0022	0.989
2	NP	0.0040	0.998
3	PTP	0.0085	0.985
4	US/NP	0.0096	0.991
5	US/PTP	0.0205	0.994

The effect of ultrasonic irradiation can be explained by dissociation of water molecules (Eq. (2)) and regeneration of  $Fe^{2+}$  from  $Fe^{3+}$  (Eq. (6)), which catalyzes Fenton reaction (Eq. (1)) to produce extra  $\cdot OH$  radicals [14]:



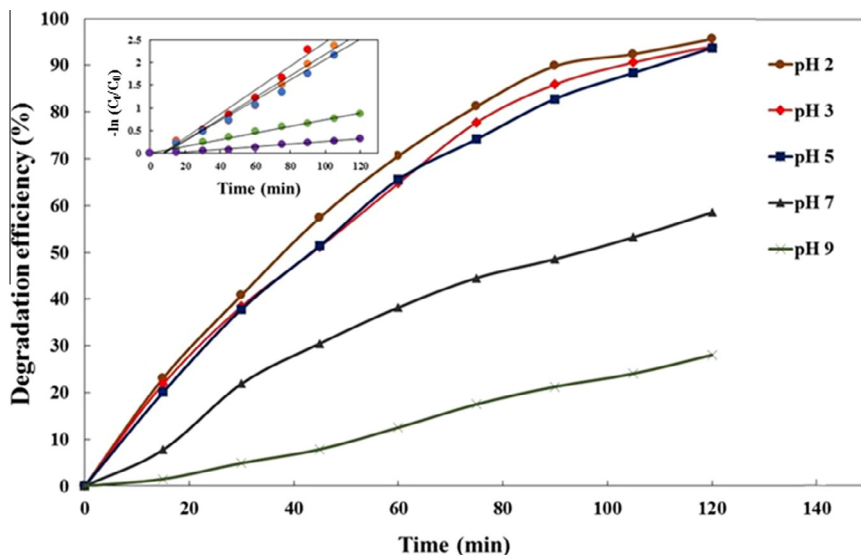


**Fig. 9.** The effect of suspension pH on the degradation efficiency of RR84 by US/PTP process;  $[RR84]_0 = 10 \text{ mg/L}$ ,  $[PTP] = 4 \text{ g/L}$ , and ultrasonic power = 300 W. The inset plot was depicted based on pseudo-first order kinetic assumption for degradation of RR84.

In addition, turbulence of the solution and solid–liquid mass transfer coefficient increase under ultrasonic waves [30]. The number of active sites on the catalyst's surface also enhance owing to deaggregation of the particles in the so; moreover, the number of cavitation microbubbles can enhance at low tensile strength of the solid–liquid interface and more cavitation nuclei in the crevices of the solid [7].

The inset of Fig. 8 revealed that all of the applied processes obey pseudo-first order kinetic; from the slope of straight lines in the inset plot, the apparent pseudo-first order rate constants ( $k_{app}$ ) for the degradation of RR84 were estimated and presented in Table 2. High correlation coefficients ( $R^2$ ), which was more than 0.98 verified the proposed kinetic.

Considerable synergistic effect of the ultrasonic irradiation and Fenton-like process using the PTP for degradation of RR84 can be expressed in the terms of the apparent pseudo-first-order rate constants through Eq. (7) [31] as 0.48:

$$\text{Synergy} = \frac{k_{US/PTP} - (k_{US} + k_{PTP})}{k_{US/PTP}} \quad (7)$$

### 3.3. Effect of the main operational parameters on the sono-Fenton-like process

The effect of main operational parameters including pH, PTP dosage, initial RR84, and ultrasonic power on the degradation of the organic pollutant was studied. pH is one of the most effective parameters in the Fenton process. Accordingly, the effect of this parameter on the degradation of RR84 was investigated, and the obtained results are shown in Fig. 9. At low pHs, high degradation efficiencies are achieved, and degradation efficiency (%) declines with increasing of the solution pH. It can be attributed to the oxidation potential of  $\cdot\text{OH}/\text{H}_2\text{O}$  redox pair, which decreases from 2.59 to 1.65 V vs. standard hydrogen electrode (SHE) by increasing the solution pH from 0 to 14 [32]. This reveals that in acidic mediums, the oxidation potential of the  $\cdot\text{OH}$  radicals for the degradation of RR84 molecules is more than natural or alkaline mediums. Moreover, based on the  $\text{pH}_{\text{pzc}}$  analysis (Fig. 7), at pH values lower than  $\text{pH}_{\text{pzc}}$ , which is 6.3, the PTP surface charge is positive. It enhances the adsorption of anionic dye molecules on its surface, and thus

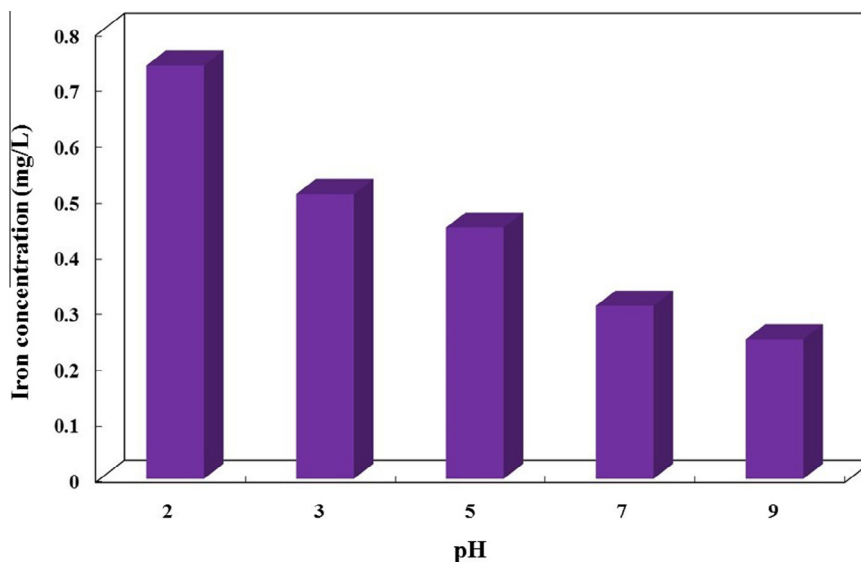


**Fig. 10.** Dissolved iron concentration in solution phase after 120 min;  $[PTP] = 4 \text{ g/L}$ .

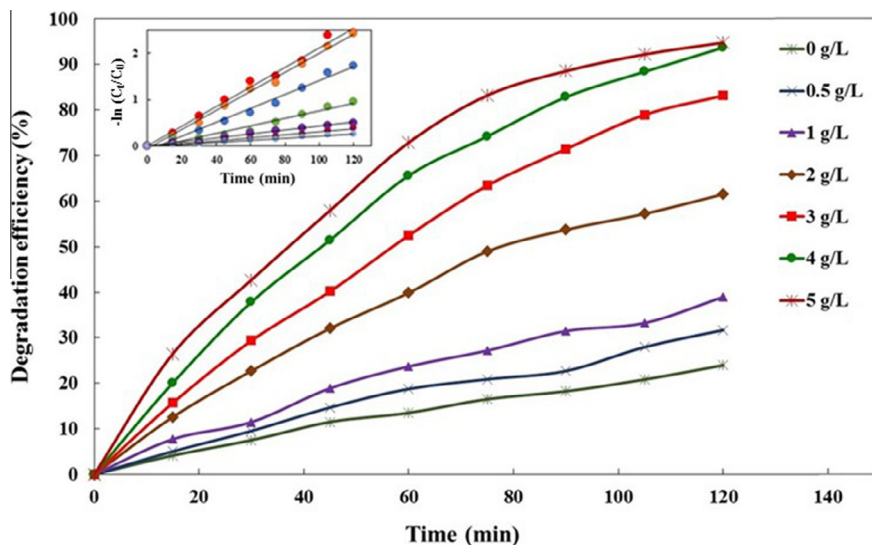


**Fig. 11.** The effect of PTP dosage on the degradation efficiency of RR84 by US/PTP process;  $[RR84]_0 = 10$  mg/L, ultrasonic power = 300 W, and pH = 5. The inset plot was depicted based on pseudo-first order kinetic assumption for degradation of RR84.

more RR84 molecules are degraded by the adsorbed reactive radicals [33,34]. Finally, to measure the total concentration of dissolved iron ions, which released into the solution at various pHs, AAS was used and the data are plotted in Fig. 10. The dissolved iron concentration increases with decreasing of the pH. Hence, high degradation is observed when the pH was adjusted in the range of 2–5, which were approximately the same. Thus, the pH 5 is selected as the optimized value. It should be mentioned that, the total leaking iron concentration is lower than 0.8 mg/L after heterogeneous sono-Fenton-like process in the presence of PTP at different pH values (Fig. 10). At this level of dissolved iron concentration, the generation of hydroxyl radicals is mainly owing to the heterogeneous sono-Fenton-like and the homogeneous Fenton reaction in the bulk solution contributed little to the degradation of RR84 [35].

Fig. 11 demonstrates the degradation of RR84 as a function of the PTP dosage in the solution, which increases from 23.8% to 93.7% after 120 min over the PTP dosage range of 0–4 g/L. This hap-

pens due to the high active sites for the reactive radical formation and adsorption [36]. Afterwards, the degradation efficiency remains almost constant owing to the scavenging effect of  $Fe^{2+}$  on the hydroxyl radicals (Eq. (8)), [37,38].



Also, screening of the ultrasonic waves by the more amount of solid particles inhibits the solution from receiving the same value of dissipated energy [39]. Since the highest degradation efficiency of RR84 is observed with 4 g/L of PTP and after that remains approximately constant after 120 min of treatment, hence, this dosage is selected as the desired amount for the rest of the experiments.

By increasing of the RR84 concentration from 10 to 40 mg/L, the degradation efficiency decreases from 93.7% to 30.5% in 120 min (Fig. 12). At the identical operational conditions, the available surface area of the PTP to adsorb dye molecules are constant, and also the same number of hydroxyl radicals were generated, accordingly,

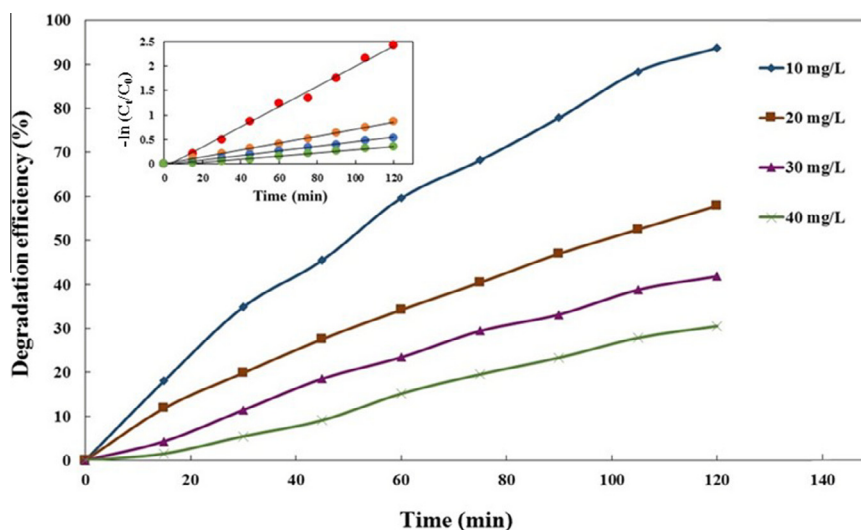


**Fig. 12.** The effect of dye concentrations on the decolorization efficiency of RR84 by US/PTP process;  $[PTP] = 4$  g/L, ultrasonic power = 300 W, and pH = 5. The inset plot was depicted based on pseudo-first order kinetic assumption for degradation of RR84.

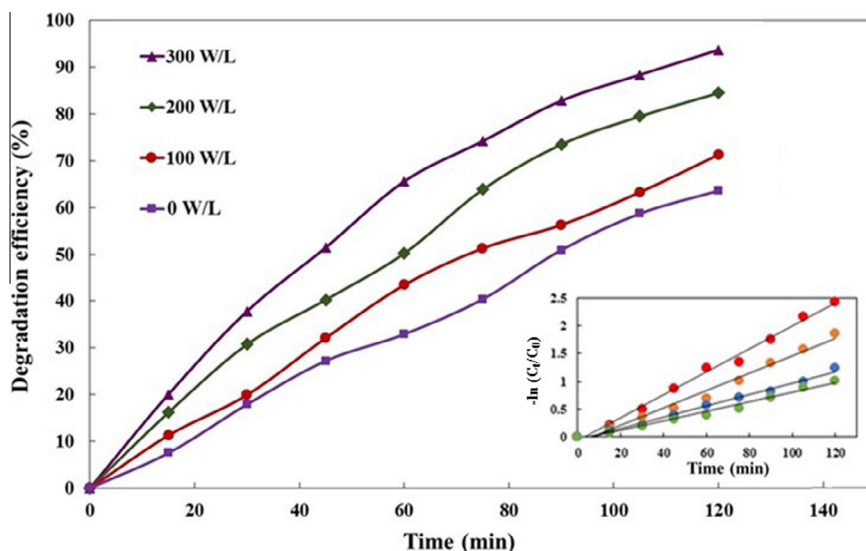


**Fig. 13.** The effect of ultrasonic power on the decolorization efficiency of RR84 by US/PTP process;  $[RR84]_0 = 10 \text{ mg/L}$ ,  $[PTP] = 4 \text{ g/L}$ , and  $\text{pH} = 5$ . The inset plot was depicted based on pseudo-first order kinetic assumption for degradation of RR84.

**Table 3**

Effect of the operational parameters on the apparent pseudo-first order constant of degradation for sono-Fenton-like process.

Operational parameters and amounts	$k_{app}$ ( $\text{min}^{-1}$ )	Correlation coefficient ( $R^2$ )
<i>pH</i>		
2	0.0264	0.985
3	0.0223	0.978
5	0.0216	0.969
7	0.0074	0.993
9	0.0029	0.986
<i>PTP dosage (g/L)</i>		
0	0.0023	0.994
0.5	0.0032	0.992
1	0.0042	0.004
2	0.0081	0.966
3	0.0153	0.986
4	0.0198	0.992
5	0.0211	0.989
<i>RR84 concentration (mg/L)</i>		
10	0.0205	0.994
20	0.0071	0.998
30	0.0047	0.997
40	0.0033	0.988
<i>Ultrasonic power</i>		
0	0.0085	0.985
100	0.0102	0.991
200	0.0145	0.976
300	0.0205	0.994

the number of RR84 molecules and their degradation intermediates that can react with hydroxyl radicals is thus constant even with increasing of the initial dye concentration [38,40,41].

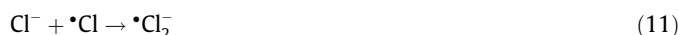
The degradation efficiency of 71.2, 84.4, and 93.7% was achieved under ultrasonic power of 100, 200 and 300 W, respectively (Fig. 13) indicating the positive effect of ultrasound intensity on the dye degradation. With increasing of the ultrasonic power, more energy is dissipated to the system, which enhances the number of cavitation bubbles and consequently reactive radicals as explained in Section 3.2.1 [42].

In all of the experiments, the degradation rate also obeys the pseudo-first order kinetics and the apparent pseudo-first-order rate constants were determined from the inset plots of Figs. 9 and 11–13 and presented in Table 3.

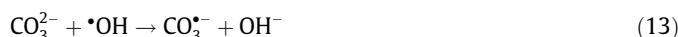
### 3.4. Effect of hydroxyl radical scavengers

Chloride, sulfate and carbonate are regular inorganic anions in textile effluents and may influence the treatment efficiency, which is called the salting-out effect. Fig. 14 indicates that the presence of these chemicals in the dye solutions decline the RR84 degradation efficiency. These negative ions are adsorbed on the positively charged surface of PTP at pH 5 and occupied active sites that contributed to the US/PTP process; this reduces the amount of  $\cdot\text{OH}$  production [43].

The effect of NaCl on the RR84 degradation was higher than that of  $\text{Na}_2\text{CO}_3$  and  $\text{Na}_2\text{SO}_4$ . This can be attributed to the scavenging of  $\cdot\text{OH}$  by chloride and the formation of reactive radicals with low oxidation potential rather than  $\cdot\text{OH}$  by the Eqs. (9)–(11) [6,41]: Furthermore, the generated  $\cdot\text{Cl}$  radicals have a great tendency to react with  $\text{H}_2\text{O}_2$ , which declines  $\cdot\text{OH}$  formation (Eq. (12)) [44].



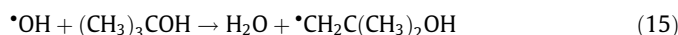
Moreover, carbonate ions may react with  $\cdot\text{OH}$  and lead to the generation of  $\text{CO}_3^{\cdot-}$  radicals with low oxidation potential (Eq. (13)). This decreases the RR84 degradation efficiency [45].



Sulfate ions can also react with  $\cdot\text{OH}$  (Eq. (14)), however, the formed  $\text{SO}_4^{\cdot-}$  radicals have oxidation potential of 2.6 V [46,47]. Hence, the scavenging effect of sulfate was declined by the  $\text{SO}_4^{\cdot-}$  radicals formation.



Finally, t-butanol as an organic  $\cdot\text{OH}$  radical scavengers was added to the RR84 solution and the degradation efficiency also decreased owing to the following reaction (Eq. (15)) [48]:



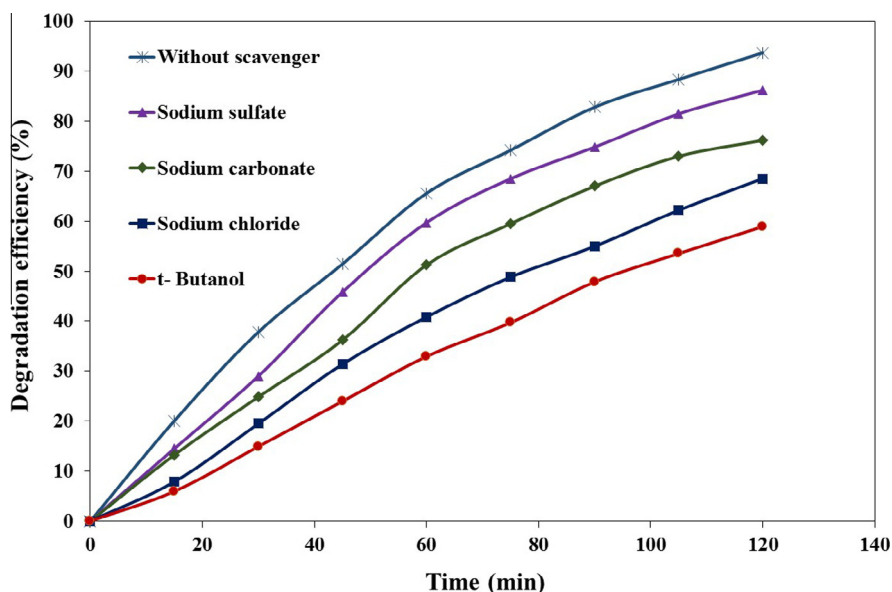


Fig. 14. Effect of scavengers on the degradation of RR84 by US/PTP process; [RR84]<sub>0</sub> = 10 mg/L, [PTP] = 4 g/L, ultrasonic power = 300 W, pH = 5, and [Scavenger]<sub>0</sub> = 10 mg/L.

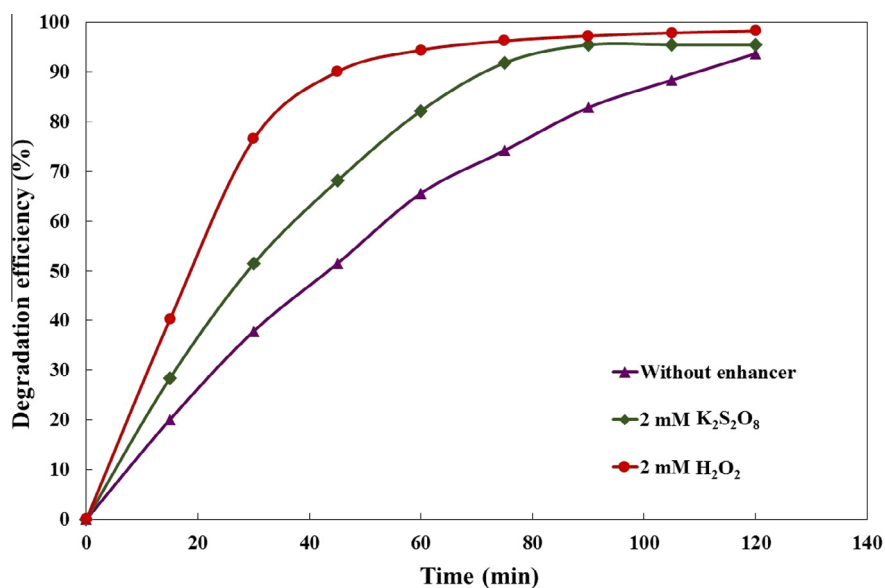


Fig. 15. Effect of the presence of hydrogen peroxide and peroxydisulfate on the degradation of RR84 by US/PTP process; [RR84]<sub>0</sub> = 10 mg/L, [PTP] = 4 g/L, ultrasonic power = 300 W, pH = 5, and [Enhancer]<sub>0</sub> = 10 mg/L.

As a consequence, the radical mechanism for the degradation of RR84 with the main role of  $\cdot\text{OH}$  radicals was confirmed, which is in consistent with other studies [49].

### 3.5. Effect of enhancers

Fig. 15 shows the effect of adding enhancers on the degradation efficiency of RR84. The enhanced degradation efficiency in the presence of  $\text{H}_2\text{O}_2$  is due to the increased formation of  $\cdot\text{OH}$  by the Fenton reaction (Eq. (1)) [50].

The peroxydisulfate anion ( $\text{S}_2\text{O}_8^{2-}$ ) effect is also studied on the RR84 degradation. This oxidant can be converted to sulfate radicals ( $\text{SO}_4^{\cdot-}$ ) in the presence of PTP as a heterogeneous catalyst (Eq. (16)), which is more powerful oxidant (2.6 V) than peroxydisulfate (2.01 V) [51]:



### 3.6. RR84 degradation intermediates

Identified compounds of RR84 degradation by US/PTP process were presented in Table 4, when the match factor of mass spectrum was above 90%. Comparison of the recognized compounds and the dye molecule indicates the conversion of RR84 to the small aromatic and aliphatic compounds, which can occur by cleavage of C–C, C–N, C–S or N=N bonds [52]. However, identification of all intermediates is not possible due to their slight accumulation and limitation related to the GC–Mass method [53].

### 3.7. Stability of PTP in successive US/PTP process

One of the most significant properties of a catalyst from practical point of view is its stability in the successive applications. Hence, the PTP was used in five repeated sono-Fenton-like

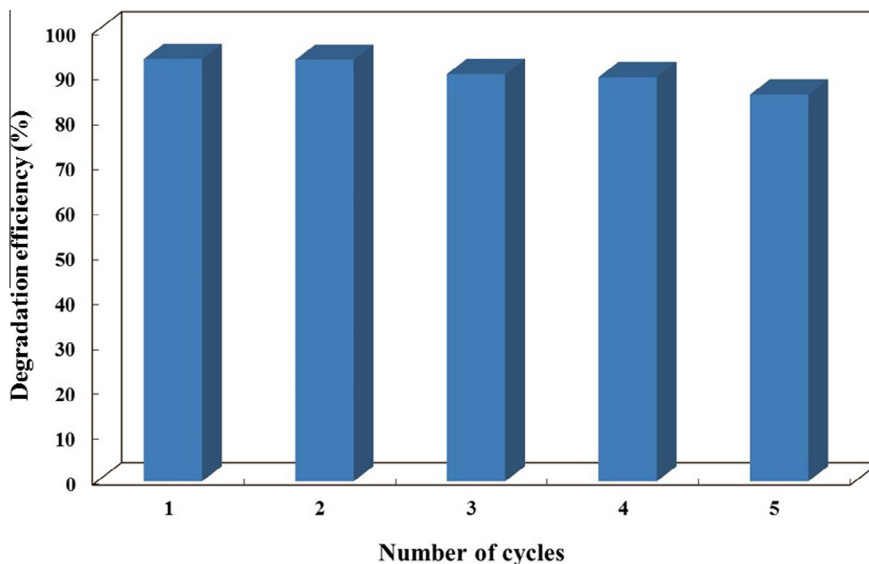


Fig. 16. Degradation efficiencies for five successive cycles;  $[RR84]_0 = 10 \text{ mg/L}$ ,  $[PTP] = 4 \text{ g/L}$ , ultrasonic power = 300 W, and  $\text{pH} = 5$ .

Table 4

Identified by-products during degradation of RR84 by sono-Fenton-like process.

No.	Compound name	Structure	Retention time (min)	Main fragments
1	$\beta$ -Naphthylamine		9.424	71, 115, 116, 143
2	Nitrobenzene		24.559	77, 51, 130
3	p-Cresol		18.625	39, 51, 77, 107
4	1,2-Benzenedicarboxylic acid		9.464	104, 76, 50
5	Hydroquinone		13.109	45, 73, 112, 239
6	Butanamide		5.106	27, 41, 44, 59
7	Butenedioic acid		7.680	43, 53, 73, 147

processes, and its function and reusability were determined. After each degradation experiment, the PTP particles were separated from the solution, washed, dried, and applied for the next experiment. The RR84 degradation efficiency for these five successive

processes is demonstrated in Fig. 16. The results reveal that the degradation efficiency was still high after several usages. Moreover, the data of released iron measurements (Fig. 10) shows that at  $\text{pH} 5$ , the dissolved iron concentration was about  $0.45 \text{ mg/L}$ . In

each degradation experiment, the PTP dosage was 4 g/L, and the main part of iron were remained in the PTP structure, so it can be noticed as stable.

#### 4. Conclusions

In this study, environmentally friendly argon plasma method was utilized successfully to produce modified pyrite, which characterized by XRD, FT-IR, BET and SEM methods. The sputtering effect of Ar glow discharge plasma results in production of the PTP nanostructures with more surface area and hence extra active sites. Furthermore, the Ar plasma can remove some of impurities from the NP surface. Consequently, The PTP performance in heterogeneous sono-Fenton-like process was improved considerably in comparison of the NP for the treatment of RR84 as a model azo dye from textile industry. The optimized operational conditions for the dye degradation were found to be PTP of 4 g/L, initial dye concentration of 10 mg/L, pH 5, and ultrasonic power of 300 W after 120 min of process time. The enhancers increase and hydroxyl radical scavengers decline the dye degradation efficiency confirming the main role of  $\cdot\text{OH}$  radicals in the degradation of the RR84 during the US/PTP process. Then, GC–Mass was used for identification of some degradation intermediates. The other significant advantages of the stable PTP are no need for adding of  $\text{H}_2\text{O}_2$ , low leached iron amount and application at the milder pH.

#### Acknowledgment

The authors thank the University of Tabriz for the support provided.

#### References

- [1] B. Ayoubi-Feiz, S. Aber, A. Khataee, E. Alipour, Electrosorption and photocatalytic one-stage combined process using a new type of nanosized  $\text{TiO}_2$ /activated charcoal plate electrode, *Environ. Sci. Pollut. Res.* 21 (2014) 8555–8564.
- [2] M. Sheydaei, S. Aber, A. Khataee, Preparation of a novel  $\gamma\text{-FeOOH-GAC}$  nano composite for decolorization of textile wastewater by photo Fenton-like process in a continuous reactor, *J. Mol. Catal. A: Chem.* 392 (2014) 229–234.
- [3] M. Sheydaei, S. Aber, A. Khataee, Degradation of amoxicillin in aqueous solution using nanolepidocrocite chips/ $\text{H}_2\text{O}_2$ /UV: optimization and kinetics studies, *J. Ind. Eng. Chem.* 20 (2013) 1772–1778.
- [4] K. Rusevova, F.-D. Kopinke, A. Georgi, Nano-sized magnetic iron oxides as catalysts for heterogeneous Fenton-like reactions – influence of  $\text{Fe(II)/Fe(III)}$  ratio on catalytic performance, *J. Hazard. Mater.* 241–242 (2012) 433–440.
- [5] A.R. Khataee, M. Zarei, A.R. Khataee, Electrochemical treatment of dye solution by oxalate catalyzed photoelectro-fenton process using a carbon nanotube-PTFE cathode: optimization by central composite design, *CLEAN Soil Air Water* 39 (2011) 482–490.
- [6] A. Khataee, M. Sheydaei, A. Hassani, M. Taseidifar, S. Karaca, Sonocatalytic removal of an organic dye using  $\text{TiO}_2$ /Montmorillonite nanocomposite, *Ultrason. Sonochem.* 22 (2015) 404–411.
- [7] C.-H. Weng, Y.-T. Lin, C.-K. Chang, N. Liu, Decolorization of direct blue 15 by Fenton/ultrasonic process using a zero-valent iron aggregate catalyst, *Ultrason. Sonochem.* 20 (2013) 970–977.
- [8] A. Khataee, A. Karimi, S. Arefi-Oskoui, R. Darvishi Cheshmeh Soltani, Y. Hanifehpour, B. Soltani, S.W. Joo, Sonochemical synthesis of Pr-doped ZnO nanoparticles for sonocatalytic degradation of Acid Red 17, *Ultrason. Sonochem.* 22 (2015) 371–381.
- [9] W. Wang, Y. Qu, B. Yang, X. Liu, W. Su, Lactate oxidation in pyrite suspension: a Fenton-like process in situ generating  $\text{H}_2\text{O}_2$ , *Chemosphere* 86 (2012) 376–382.
- [10] X. Liang, Y. Zhong, H. He, P. Yuan, J. Zhu, S. Zhu, Z. Jiang, The application of chromium substituted magnetite as heterogeneous Fenton catalyst for the degradation of aqueous cationic and anionic dyes, *Chem. Eng. J.* 191 (2012) 177–184.
- [11] Z.-R. Lin, L. Zhao, Y.-H. Dong, Quantitative characterization of hydroxyl radical generation in a goethite-catalyzed Fenton-like reaction, *Chemosphere* 141 (2015) 7–12.
- [12] Y. Zhang, K. Zhang, C. Dai, X. Zhou, H. Si, An enhanced Fenton reaction catalyzed by natural heterogeneous pyrite for nitrobenzene degradation in an aqueous solution, *Chem. Eng. J.* 244 (2014) 438–445.
- [13] S. Bae, D. Kim, W. Lee, Degradation of diclofenac by pyrite catalyzed Fenton oxidation, *Appl. Catal. B* 134–135 (2013) 93–102.
- [14] M. Sheydaei, A. Khataee, Sonocatalytic decolorization of textile wastewater using synthesized  $\gamma\text{-FeOOH}$  nanoparticles, *Ultrason. Sonochem.* 27 (2015) 616–622.
- [15] X. Zhang, W.-J. Sun, W. Chu, Effect of glow discharge plasma treatment on the performance of Ni/ $\text{SiO}_2$  catalyst in  $\text{CO}_2$  methanation, *J. Fuel Chem. Technol.* 41 (2013) 96–101.
- [16] A. Khataee, S. Bozorg, S. Khorram, M. Fathinia, Y. Hanifehpour, S.W. Joo, Conversion of natural clinoptilolite microparticles to nanorods by glow discharge plasma: a novel Fe-impregnated nanocatalyst for the heterogeneous fenton process, *Ind. Eng. Chem. Res.* 52 (2013) 18225–18233.
- [17] P. Attri, B. Arora, E.H. Choi, Utility of plasma: a new road from physics to chemistry, *RSC Adv.* 3 (2013) 12540–12567.
- [18] C.-J. Liu, K. Yu, Y.-P. Zhang, X. Zhu, F. He, B. Eliasson, Characterization of plasma treated Pd/HZSM-5 catalyst for methane combustion, *Appl. Catal. B* 47 (2004) 95–100.
- [19] Y. Li, B.W.L. Jang, Non-thermal RF plasma effects on surface properties of Pd/ $\text{TiO}_2$  catalysts for selective hydrogenation of acetylene, *Appl. Catal. A* 392 (2011) 173–179.
- [20] M. Taseidifar, A. Khataee, B. Vahid, S. Khorram, S.W. Joo, Production of nanocatalyst from natural magnetite by glow discharge plasma for enhanced catalytic ozonation of an oxazine dye in aqueous solution, *J. Mol. Catal. A: Chem.* 404–405 (2015) 218–226.
- [21] S. Liu, M. Li, S. Li, H. Li, L. Yan, Synthesis and adsorption/photocatalysis performance of pyrite  $\text{FeS}_2$ , *Appl. Surf. Sci.* 268 (2013) 213–217.
- [22] S.A. Stanley, C. Stuttle, A.J. Caruana, M.D. Cropper, A.S.O. Walton, An investigation of the growth of bismuth whiskers and nanowires during physical vapour deposition, *J. Phys. D Appl. Phys.* 45 (2012) 435304.
- [23] S. Fathinia, M. Fathinia, A.A. Rahmani, A. Khataee, Preparation of natural pyrite nanoparticles with high energy planetary ball milling as a nanocatalyst for heterogeneous Fenton process, *Appl. Surf. Sci.* 327 (2015) 190–200.
- [24] Y. Bi, Y. Yuan, C.L. Exstrom, S.A. Darveau, J. Huang, Air stable, photosensitive, phase pure iron pyrite nanocrystal thin films for photovoltaic application, *Nano Lett.* 11 (2011) 4953–4957.
- [25] R. Ashiri, Detailed FT-IR spectroscopy characterization and thermal analysis of synthesis of barium titanate nanoscale particles through a newly developed process, *Vib. Spectrosc.* 66 (2013) 24–29.
- [26] B.O. Aronsson, J. Lausmaa, B. Kasemo, Glow discharge plasma treatment for surface cleaning and modification of metallic biomaterials, *J. Biomed. Mater. Res.* 35 (1997) 49–73.
- [27] S. Aber, M. Sheydaei, Removal of COD from industrial effluent containing indigo dye using adsorption method by activated carbon cloth: optimization, kinetic, and isotherm studies, *Clean Soil Air Water* 40 (2012) 87–94.
- [28] A. Khataee, M. Taseidifar, S. Khorram, M. Sheydaei, S.W. Joo, Preparation of nanostructured magnetite with plasma for degradation of a cationic textile dye by the heterogeneous Fenton process, *J. Taiwan Inst. Chem. E.* 53 (2015) 132–139.
- [29] M.A.A. Schoonen, A.D. Harrington, R. Laffers, D.R. Strongin, Role of hydrogen peroxide and hydroxyl radical in pyrite oxidation by molecular oxygen, *Geochim. Cosmochim. Acta* 74 (2010) 4971–4987.
- [30] K.R. Reddy, W. Park, B.C. Sin, J. Noh, Y. Lee, Synthesis of electrically conductive and superparamagnetic monodispersed iron oxide-conjugated polymer composite nanoparticles by in situ chemical oxidative polymerization, *J. Colloid Interface Sci.* 335 (2009) 34–39.
- [31] M. Behnajady, N. Modirshahla, M. Shokri, B. Vahid, Investigation of the effect of ultrasonic waves on the enhancement of efficiency of direct photolysis and photooxidation processes on the removal of a model contaminant from textile industry, *Global Nest J.* 10 (2008) 8–15.
- [32] A. Babuponnusami, K. Muthukumar, A review on Fenton and improvements to the Fenton process for wastewater treatment, *J. Environ. Chem. Eng.* 2 (2014) 557–572.
- [33] S. Mustafa, B. Dilara, K. Nargis, A. Naeem, P. Shahida, Surface properties of the mixed oxides of iron and silica, *Colloids Surf., A* 205 (2002) 273–282.
- [34] S. Aber, A. Khataee, M. Sheydaei, Optimization of activated carbon fiber preparation from Kenaf using  $\text{K}_2\text{HPO}_4$  as chemical activator for adsorption of phenolic compounds, *Bioresour. Technol.* 100 (2009) 6586–6591.
- [35] Z. Xu, J. Liang, L. Zhou, Photo-Fenton-like degradation of azo dye methyl orange using synthetic ammonium and hydronium jarosite, *J. Alloy. Compd.* 546 (2013) 112–118.
- [36] X. Zhang, Y. Ding, H. Tang, X. Han, L. Zhu, N. Wang, Degradation of bisphenol A by hydrogen peroxide activated with  $\text{CuFeO}_2$  microparticles as a heterogeneous Fenton-like catalyst: efficiency, stability and mechanism, *Chem. Eng. J.* 236 (2014) 251–262.
- [37] Y. Kuang, Q. Wang, Z. Chen, M. Megharaj, R. Naidu, Heterogeneous Fenton-like oxidation of monochlorobenzene using green synthesis of iron nanoparticles, *J. Colloid Interface Sci.* 410 (2013) 67–73.
- [38] S.-P. Sun, A.T. Lemley, P-Nitrophenol degradation by a heterogeneous Fenton-like reaction on nano-magnetite: process optimization, kinetics, and degradation pathways, *J. Mol. Catal. A: Chem.* 349 (2011) 71–79.
- [39] B. Vahid, T. Mousanejad, A. Khataee, Sonocatalytic ozonation, with nano- $\text{TiO}_2$  as catalyst, for degradation of 4-chloronitrobenzene in aqueous solution, *Res. Chem. Intermed.* (2014) 1–14.
- [40] M. Neam u, C. Zaharia, C. Catrinescu, A. Yediler, M. Macoveanu, A. Kettrup, Fe-exchanged Y zeolite as catalyst for wet peroxide oxidation of reactive azo dye Procion Marine H-EXL, *Appl. Catal. B: Environ.* 48 (2004) 287–294.
- [41] B.G. Kwon, D.S. Lee, N. Kang, J. Yoon, Characteristics of p-chlorophenol oxidation by Fenton's reagent, *Water Res.* 33 (1999) 2110–2118.
- [42] A.M. Atta, O.E. El-Azabawy, H.S. Ismail, M.A. Hegazy, Novel dispersed magnetite core-shell nanogel polymers as corrosion inhibitors for carbon steel in acidic medium, *Corros. Sci.* 53 (2011) 1680–1689.

- [43] A. Khataee, R.D.C. Soltani, A. Karimi, S.W. Joo, Sonocatalytic degradation of a textile dye over Gd-doped ZnO nanoparticles synthesized through sonochemical process, *Ultrason. Sonochem.* 23 (2015) 219–230.
- [44] M. Ortega-Liébana, E. Sánchez-López, J. Hidalgo-Carrillo, A. Marinas, J. Marinas, F. Urbano, A comparative study of photocatalytic degradation of 3-chloropyridine under UV and solar light by homogeneous (photo-Fenton) and heterogeneous (TiO<sub>2</sub>) photocatalysis, *Appl. Catal. B* 127 (2012) 316–322.
- [45] A. Khataee, A. Khataee, M. Fathinia, Y. Hanifehpour, S.W. Joo, Kinetics and mechanism of enhanced photocatalytic activity under visible light using synthesized Pr<sub>x</sub>Cd<sub>1-x</sub>Se nanoparticles, *Ind. Eng. Chem. Res.* 52 (2013) 13357–13369.
- [46] R. Soltani, A. Rezaee, A. Khataee, M. Safari, Photocatalytic process by immobilized carbon black/ZnO nanocomposite for dye removal from aqueous medium: optimization by response surface methodology, *J. Ind. Eng. Chem.* 20 (2014) 1861–1868.
- [47] C. Deng, H. Hu, X. Ge, C. Han, D. Zhao, G. Shao, One-pot sonochemical fabrication of hierarchical hollow CuO microspheres, *Ultrason. Sonochem.* 18 (2011) 932–937.
- [48] H. Zhao, G. Zhang, Q. Zhang, MnO<sub>2</sub>/CeO<sub>2</sub> for catalytic ultrasonic degradation of methyl orange, *Ultrason. Sonochem.* 21 (2014) 991–996.
- [49] Z. Frontistis, D. Mantzavinos, Sonodegradation of 17 $\alpha$ -ethynylestradiol in environmentally relevant matrices: laboratory-scale kinetic studies, *Ultrason. Sonochem.* 19 (2012) 77–84.
- [50] L. Xu, J. Wang, Fenton-like degradation of 2,4-dichlorophenol using Fe<sub>3</sub>O<sub>4</sub> magnetic nanoparticles, *Appl. Catal. B* 123–124 (2012) 117–126.
- [51] I. Velo-Gala, J.J. López-Peñalver, M. Sánchez-Polo, J. Rivera-Utrilla, Comparative study of oxidative degradation of sodium diatrizoate in aqueous solution by H<sub>2</sub>O<sub>2</sub>/Fe<sup>2+</sup>, H<sub>2</sub>O<sub>2</sub>/Fe<sup>3+</sup>, Fe (VI) and UV, H<sub>2</sub>O<sub>2</sub>/UV, K<sub>2</sub>S<sub>2</sub>O<sub>8</sub>/UV, *Chem. Eng. J.* 241 (2014) 504–512.
- [52] C.-Y. Chen, Photocatalytic degradation of azo dye reactive orange 16 by TiO<sub>2</sub>, *Water Air Soil Pollut.* 202 (2009) 335–342.
- [53] A.R. Khataee, M. Safarpour, M. Zarei, S. Aber, Combined heterogeneous and homogeneous photodegradation of a dye using immobilized TiO<sub>2</sub> nanophotocatalyst and modified graphite electrode with carbon nanotubes, *J. Mol. Catal. A: Chem.* 363–364 (2012) 58–68.